Circulation Research
JOURNAL OF THE AMERICAN HEART ASSOCIATION

Abnormal Propagation of Calcium Waves and Ultrastructural Remodeling in Recessive Catecholaminergic Polymorphic Ventricular TachycardiaNovelty and Significance

Nian Liu, Marco Denegri, Wen Dun, Simona Boncompagni, Francesco Lodola, Feliciano Protasi, Carlo Napolitano, Penelope A. Boyden and Silvia G. Priori

Circ Res. 2013;113:142-152; originally published online May 14, 2013;
doi: 10.1161/CIRCRESAHA.113.301783
Circulation Research is published by the American Heart Association, 7272 Greenville Avenue, Dallas, TX 75231

Print ISSN: 0009-7330. Online ISSN: 1524-4571

Abnormal Propagation of Calcium Waves and Ultrastructural Remodeling in Recessive Catecholaminergic Polymorphic Ventricular Tachycardia

Nian Liu, Marco Denegri, Wen Dun, Simona Boncompagni, Francesco Lodola, Feliciano Protasi, Carlo Napolitano, Penelope A. Boyden,* Silvia G. Priori*

Rationale: **The recessive form of catecholaminergic polymorphic ventricular tachycardia is caused by mutations in the cardiac calsequestrin-2 gene; this variant of catecholaminergic polymorphic ventricular tachycardia is less well characterized than the autosomal-dominant form caused by mutations in the ryanodine receptor-2 gene.**

Objective: **We characterized the intracellular Ca^{2+} homeostasis, electrophysiological properties, and ultrastructural features of the Ca^{2+} release units in the homozygous calsequestrin 2-R33Q knock-in mouse model (R33Q) R33Q knock-in mouse model.**

Methods and Results: **We studied isolated R33Q and wild-type ventricular myocytes and observed properties not previously identified in a catecholaminergic polymorphic ventricular tachycardia model. As compared with wild-type cells, R33Q myocytes (1) show spontaneous Ca^{2+} waves unable to propagate as cell-wide waves; (2) show smaller Ca^{2+}sparks with shortened coupling intervals, suggesting a reduced refractoriness of Ca^{2+} release events; (3) have a reduction of the area of membrane contact, of the junctions between junctional sarcoplasmic reticulum and T tubules (couplons), and of junctional sarcoplasmic reticulum volume; (4) have a propensity to develop phase 2 to 4 afterdepolarizations that can elicit triggered beats; and (5) involve viral gene transfer with wild-type cardiac calsequestrin-2 that is able to normalize structural abnormalities and to restore cell-wide calcium wave propagation.**

Conclusions: **Our data show that homozygous cardiac calsequestrin-2–R33Q myocytes develop spontaneous Ca^{2+} release events with a broad range of intervals coupled to preceding beats, leading to the formation of early and delayed afterdepolarizations. They also display a major disruption of the Ca^{2+} release unit architecture that leads to fragmentation of spontaneous Ca^{2+} waves. We propose that these 2 substrates in R33Q myocytes synergize to provide a new arrhythmogenic mechanism for catecholaminergic polymorphic ventricular tachycardia. (*Circ Res*. 2013;113:142-152.)**

Key Words: arrhythmias ■ calcium ■ calsequestrin ■ cardiomyopathies ■ chronic disease ■ electrophysiology ■ genetic diseases

Catecholaminergic polymorphic ventricular tachycardia (CPVT) is an inherited arrhythmogenic disease characterized by stress- and emotion-induced life-threatening arrhythmias. Mutations in the cardiac ryanodine receptor-2 (*RyR2*) and cardiac calsequestrin-2 (*CASQ2*) genes have been associated with the autosomal-dominant and the autosomal-recessive forms of CPVT.[1] Knock-in mouse models that carry gain-of-function *RyR2* mutations exhibit phenotypes similar to the clinical manifestations observed in patients with CPVT, including the development of bidirectional/polymorphic VT on exposure to catecholamines.[2–5] Investigations of knock-in models of dominant CPVT have demonstrated that abnormal Ca^{2+} release from mutant RyR2 induces cell-wide Ca^{2+} waves, delayed afterdepolarizations (DADs) and triggered activity, all of which are arrhythmogenic.[2,4,6]

Recently, attention has turned to the study of the recessive form of CPVT that is caused by homozygous mutations in the *CASQ2* gene. Most experimental studies on recessive CPVT have been performed using CASQ2 knockout mice, whereas only few knock-in mouse carriers of human *CASQ2* mutations

Original received May 4, 2013; revision received May 13, 2013; accepted May 14, 2013. In April 2013, the average time from submission to first decision for all original research papers submitted to *Circulation Research* was 13.5 days.

From the Leon H. Charney Division of Cardiology, Cardiovascular Genetics Program, New York University School of Medicine, New York, NY (N.L., C.N., S.G.P.); Department of Molecular Cardiology, IRCCS Fondazione Salvatore Maugeri, Pavia, Italy (M.D., F.L., C.N., S.G.P.); Department of Molecular Medicine, University of Pavia, Pavia, Italy (S.G.P.); Center for Research on Ageing and Department of Neuroscience and Imaging, G. d'Annunzio University, Chieti, Italy (S.B., F.P.); and Department of Pharmacology, Columbia College of Physicians and Surgeons, New York, NY (W.D., P.A.B.).

This manuscript was sent to Gordon Tomaselli, Consulting Editor, for review by expert referees, editorial decision, and final disposition.

*These authors contributed equally.

The online-only Data Supplement is available with this article at http://circres.ahajournals.org/lookup/suppl/doi:10.1161/CIRCRESAHA.113.301783/-/DC1.

Correspondence to Silvia G. Priori, Cardiovascular Genetics Program, Leon H. Charney Division of Cardiology, New York University School of Medicine, Smilow Research Bldg, Room 701, 522 First Ave, New York, NY. E-mail silvia.priori@nyumc.org

Circulation Research **is available at http://circres.ahajournals.org** **DOI: 10.1161/CIRCRESAHA.113.301783**

Nonstandard Abbreviations and Acronyms	
CASQ2	cardiac calsequestrin-2
CASQ2-AAV9	adeno-associated viral construct containing CASQ2 DNA
CICR	Ca^{2+}-induced Ca^{2+} release
CPVT	catecholaminergic polymorphic ventricular tachycardia
CRU	Ca^{2+} release unit
DAD	delayed afterdepolarization
EAD	early afterdepolarization
Iso	isoproterenol
jSR	junctional sarcoplasmic reticulum
RyR2	ryanodine receptor-2
SCaE	spontaneous Ca^{2+} release events
SR	sarcoplasmic reticulum
TT	T tubule
VT	ventricular tachycardia
WT	wild-type

have been characterized.[7–9] As a consequence, the pathophysiology of arrhythmias generated by *CASQ2* missense mutations remains only partially characterized.

Here, we investigate the Ca^{2+} homeostasis/dynamics, cellular electrophysiology, and ultrastructure of the Ca^{2+} release units (CRUs) in the knock-in mouse model of the recessive CPVT carrier of the homozygous R33Q CASQ2 missense mutation that presents with severe adrenergically induced bidirectional and polymorphic ventricular arrhythmias.[8] Our data identify a unique profile that differs from that previously reported in CPVT mouse models. Specifically, we observe that spontaneous Ca^{2+} release events (SCaEs) in intact R33Q myocytes are characterized by (1) the development of fragmented wavelets that often are unable to generate cell-wide waves, (2) the simultaneous occurrence of early afterdepolarization (EADs) and DADs, and (3) oscillations of the resting membrane potential. This abnormal behavior is accompanied by profound ultrastructural remodeling of the CRUs. We propose that the abnormal architecture of CRUs in the presence of a high likelihood of SCaEs resulting from the loss of CASQ2 creates an electrically unstable arrhythmogenic background that, to date, is unique to this CPVT model.

Methods

An expanded Methods section can be found in the Online Data Supplement.

Isolation of Adult Mice Ventricular Myocytes

Ventricular myocytes were isolated with an established enzymatic digestion protocol and then used for Ca^{2+} measurement or for cellular electrophysiology.[2]

Ca^{2+} Measurements

Isolated ventricular myocytes were incubated with 2.5 μmol/L Fluo-4 AM (Invitrogen Inc, Eugene, OR). Fluorescent signals were acquired using a ×40 ultraviolet fluorescence objective (numeric aperture 1.0, Nikon), and single-excitation-wavelength microfluorimetry was performed using a photomultiplier tube system (IonOptix Corp, Milton, MA). Cells were field stimulated (voltage 25% above threshold). SCaEs were defined as nonstimulated increases in intracellular Ca^{2+} and were quantified during the 5-second unpaced interval after train pacing. Sarcoplasmic reticulum (SR) Ca^{2+} load was measured as the amplitude of the 10-mmol/L caffeine-induced Ca^{2+} transient. Local spontaneous Ca^{2+} events were also measured using 2-dimensional (2D) spinning disk (Nipkow) confocal microscopy and line-scan microscopy (Online Data Supplement). Permeabilized myocytes were obtained by incubating cells with 0.01% saponin for 1.5 minutes. Free $[Ca]^{2+}_i$ was calculated by WINMAXC32 2.51. The dye was excited at 488 nm, and emission was collected at >510 nm. Image analyses were performed with spark master in Imaging J software.[10] The calcium measurements in permeabilized myocytes from mice infected with wild-type (WT) CASQ2 were performed using 1-[2-amino-5-(3-dimethylamino-6-dimethylammonio-9-xanthenyl)phenoxy]-2-(2-amino-5-methylphenoxy)ethane-N,N,N',N'-tetraacetic acid, tetraacetoxymethyl ester, chloride (Rhod-2) to avoid imaging interference with the green fluorescent protein tag of the CASQ2 construct. Rhod-2 was excited at 543 nm, and emission was collected at >560 nm.

Electrophysiological Recordings in Isolated Ventricular Myocytes

Transmembrane potentials were recorded in whole-cell mode using a multiClamp 700B amplifier (Axon Instruments). Myocytes were electrically stimulated by intracellular current injection through patch electrodes using depolarizing pulses. DADs were defined as phase 4 positive (depolarizing) deflections of the membrane potential. EADs were defined as positive (depolarizing) oscillations occurring during phase 2 or 3 of action potential. Triggered activity was defined as a nonstimulated action potential developing from a DAD or an EAD. The liquid junction potential between pipette and bath solution was calculated with pCLAMP software and corrected after experiments.

Electron Microscopy

The hearts were fixed by retrograde aortic perfusion using 3.5% glutaraldehyde in 0.1 mol/L NaCaCo buffer, pH 7.2. In each sample group (R33Q and WT), 3 hearts were fixed and analyzed.[8,11] Small bundles of cells teased from the papillary muscles were then postfixed in 2% OsO_4 in NaCaCo buffer for 2 hours and block stained in saturated uranyl acetate. After dehydration, specimens were embedded in an epoxy resin (Epon 812). Ultrathin sections were cut using a Leica Ultracut R microtome (Leica Microsystem, Austria) with a Diatome diamond knife (DiatomeLtd CH-2501 Biel, Switzerland) and double stained with uranyl acetate and lead citrate. Sections were viewed in a Morgagni Series 268D electron microscope (FEI Company, Brno, Czech Republic) equipped with Megaview III digital camera. The ultrastructural morphometry of CRUs was performed as detailed in the Online Data Supplement. Junctional SR (jSR) volume was calculated by the well-established stereology point counting technique[12] in electron micrographs taken at ×24 000 from cross sections of papillary cardiomyocytes. In each fiber, 2 or 3 pictures were taken in internal areas of the fibers, excluding the nuclei regions. The images were then covered with an orthogonal array of dots (spacing=0.17 μm). The ratio of the number of dots falling over the jSR to the total number of dots covering the entire micrograph was used to calculate the percentage of fiber volume occupied by jSR in WT and R33Q.

Viral Construct and In Vivo Infection Procedure

The adeno-associated viral serotype 9 (AAV9) vector containing the cDNA of the murine *CASQ2* gene, under the control of the cytomegalovirus promoter and followed by the enhanced green fluorescent protein as reporter gene, was produced, purified, and titered as previously described.[11] Infection of $CASQ2^{R33Q/R33Q}$ mice with AAV9 viral particles (100 μL) was performed by intraperitoneal injection on postnatal day 3. After 6 months, animals were euthanized by cervical dislocation. Cells were made for study, and tissues were prepared as above.

Data Analysis

Data were expressed as mean±SEM unless otherwise specified. A Student *t* test or a Mann–Whitney rank-sum test was used to determine statistical significance between 2 groups. One-way ANOVA with the Tukey test for post hoc subgroup analyses was used for multiple comparisons. The χ^2 and Fisher exact test were used as appropriate. Differences with $P \leq 0.05$ were considered statistically significant.

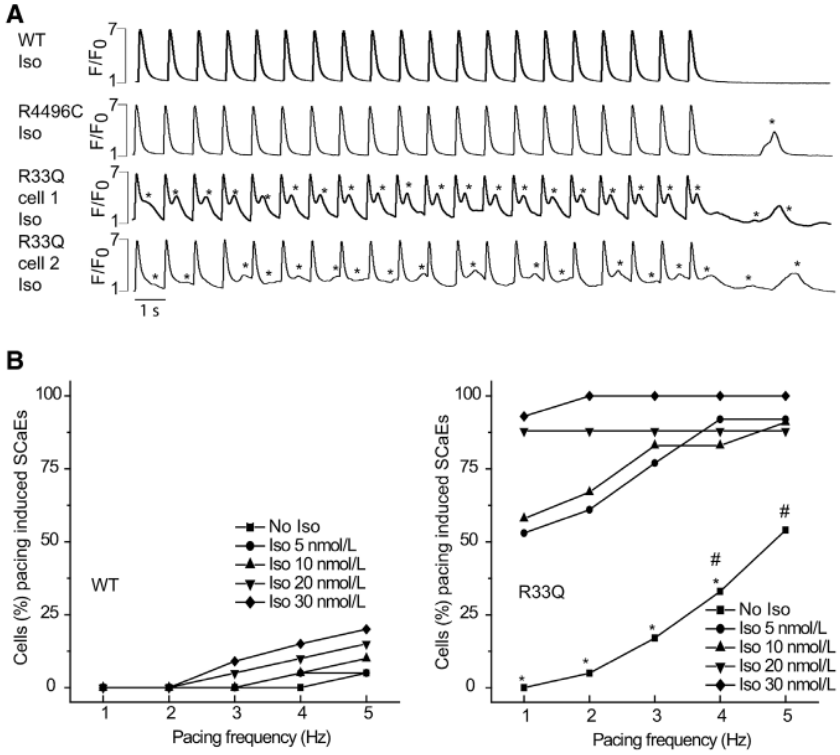

Figure 1. A, Spontaneous Ca^{2+} release events (SCaEs) elicited by field stimulation (1 Hz) in wild-type (WT), $RyR2^{R4496C+/-}$, and R33Q myocytes incubated with isoproterenol (Iso; 30 nmol/L). Only R33Q myocytes presented frequent SCaEs (*) and showed an early phase of spontaneous Ca^{2+} release; after pacing cessation, multiple Ca^{2+} oscillations often occurred. B, Relative occurrence of SCaEs in WT and R33Q myocytes incubated with increasing concentrations of Iso (5, 10, 20, and 30 nmol/L) on cessation of 1- to 5-Hz stimulation (n=12–18 cells for each group). *P<0.01 with respect to Iso-treated cells at the same pacing frequency; #P<0.01 with no Iso cells at 1-Hz pacing.

Results

Characteristics of Electrically Evoked Ca^{2+} Transients in R33Q Myocytes

We first characterized paced macroscopic Ca^{2+} transients in WT and R33Q myocytes isolated from the hearts of age-matched mice. Figure 1A shows Ca^{2+} transients of ventricular myocytes paced at 1 Hz in the presence of 30 nmol/L isoproterenol (Iso). As expected, the development of SCaEs (asterisks) in R33Q CASQ2 cells was influenced by the pacing frequency (Figure 1B, right). In the absence of Iso at 5-Hz pacing, 50% of R33Q myocytes showed SCaEs (P<0.01 versus 1 Hz), whereas in the presence of Iso 30 nmol/L at 1 Hz, 90% of R33Q cells presented SCaEs. Interestingly, SCaEs in R33Q myocytes were tightly coupled to the paced beats often during the diastolic intervals between paced beats (Figure 1A, R33Q cells 1 and 2). Notably, SCaEs occurring during diastolic intervals were not seen in cells dispersed from our autosomal-dominant CPVT mouse hearts ($RyR2^{R4496C+/-}$; Figure 1A).

Characteristics of Ca^{2+} Transients

During 0.2-Hz pacing, the amplitudes of global Ca^{2+} transients in R33Q myocytes were significantly reduced as compared with that of WT myocytes (P<0.05; Online Figure IA and IB), whereas in the presence of 30 nmol/L Iso, this difference was not significant (Online Figure IB). The average time to peak of SCaEs was identical in R33Q compared with WT myocytes in the absence or in the presence of Iso (Online Figure IC). The Ca^{2+} transient decay was significantly slower in R33Q cells compared with WT either in the absence or in the presence of Iso (P<0.05; Online Figure ID). Some may suggest a reduced sarco-endoplasmatic reticulum calcium ATPase function in R33Q cells, which would be consistent with recent observations in CASQ2 knockout and CASQ2 D307H myocytes.[13] Unexpectedly, the SR Ca^{2+} content measured as caffeine-induced Ca^{2+} transient was similar in WT and R33Q myocytes in the absence of Iso, but on exposure to 30 nmol/L Iso, it significantly increased in both cell groups, yet the increase was less pronounced in R33Q cells (P<0.05; Online Figure IE). We hypothesized that this effect may reflect greater spontaneous Ca^{2+} release activity in R33Q myocytes compared with WT in the presence of Iso. Finally, we compared the exponential time constant of Ca^{2+} decay of caffeine-induced Ca^{2+} transients to evaluate the Na^{+}/Ca^{2+} exchanger and observed no significant difference between WT and R33Q myocytes (Online Figure IF).

Ca^{2+} Sparks in WT and R33Q Ventricular Myocytes

We characterized the properties of nonpropagating Ca^{2+} sparks in WT and R33Q permeabilized myocytes (50 nmol/L $[Ca]^{2+}_i$). Ca^{2+} sparks developing in R33Q myocytes occurred with higher frequency than in WT cells; they had smaller amplitude (R33Q, 0.33±0.01 $\Delta F/F_0$ versus WT, 0.78±0.02 $\Delta F/F_0$; P<0.01), were narrower, and presented with a slower decay than WT counterparts (Figure 2A; Table 1). We calculated mass of sparks and showed that it is significantly reduced in R33Q myocytes as compared with WT cells (Table 1). Figure 2A illustrates representative Ca^{2+} spark recordings and linear profiles in WT and R33Q cells. Of note, Ca^{2+} sparks presented with various amplitudes and morphologies at the same site (hot spot site; Figure 2A, R33Q cell 1). We also noticed clusters of long-lasting spontaneous Ca^{2+} sparks (Figure 2A, R33Q cell 3, R33Q cell 4, line a). We quantified the spark-to-spark coupling intervals within these spots as an indicator of the refractoriness of SR Ca^{2+} release.[14] Figure 2B

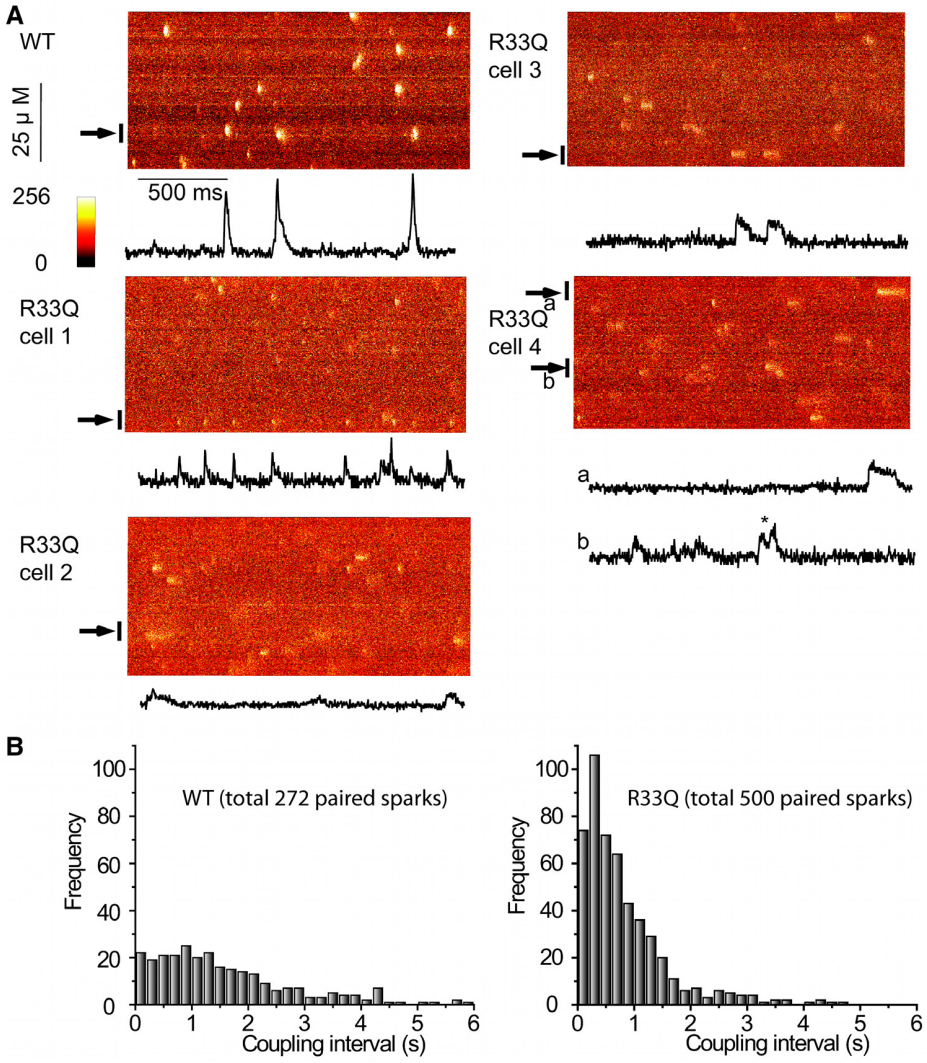

Figure 2. A, Representative confocal line-scan images of Ca^{2+} spark in permeabilized wild-type (WT) and R33Q myocytes ($[Ca]^{2+}_i$ 50 nmol/L, EGTA 0.5 mmol/L). R33Q myocyte showed variable spontaneous Ca^{2+} sparks. Cell 1: hot spot, repetitive Ca^{2+} sparks with small amplitude. Cell 2: low-amplitude sparks with slow rise and decay. Cell 3: repetitive, long-lasting sparks. Cell 4: long-lasting spark (a) and spark triggering additional spark in immediate vicinity (b, *). B, Histogram of spark-to-spark coupling interval. The histogram of spark-to-spark coupling interval in R33Q myocytes (n=10 cells) was shifted to the left compared with that observed in WT (n=10 cells) myocytes. Coupling intervals of spark events measured are shown by black bars. They are by no means measured at the level of a single micron.

shows that the histogram of spark-to-spark coupling intervals is shifted to the left in R33Q myocytes (500 paired sparks; mean, 0.82±0.03 second; $P<0.001$ versus WT) as compared with WT myocytes (272 paired sparks; mean, 1.57±0.07 seconds). A total of 71.8% of spark coupling intervals in R33Q myocytes were <1 second. Evidence of a reduced spark-to-spark coupling interval may be the consequence of a reduced refractoriness of SR Ca^{2+} release that is known to occur when CASQ2 levels are diminished.[15]

Ca^{2+}Waves in R33Q Ventricular Myocytes

We compared the characteristics of Iso-induced spontaneous Ca^{2+} release in intact WT and R33Q myocytes using high-resolution line-scan confocal microscopy. When WT myocytes

Table 1. Characterization of Ca^{2+} Sparks in Permeabilized Myocytes ($[Ca]^{2+}_i$ 50 nmol/L)

Parameters	WT (n=1302)	R33Q (n=1491)
Spark frequency, per 100 μmol/L per second	16.9□0.8	19.2□0.9*
Amplitude, $\Delta F/F_0$	0.78□0.02	0.34□0.01*
FWHM, μm	2.0□0.02	1.59□0.01*
FDHM, ms	19.6□0.2	26.9□0.4*
τ, ms	17.2□0.28	30.0□0.86*
Spark mass, $(\Delta F/F_0)$μmol/L	1.80□0.05	0.61□0.01*

Data were collected from permeabilized WT myocytes (n=23 cells from 3 mice) and R33Q myocytes (n=28 cells from 3 mice). n=number of sparks. Spark mass was calculated as amplitude□1.206□FWHM. FDHM indicates spark duration at half-maximum amplitude; FWHM, spark full-width at half-maximum amplitude; τ, exponential time constant of the spark decay; and WT, wild-type.

*P<0.01 vs WT (Mann-Whitney rank sum test).

(n=7) were exposed to Iso (100 nmol/L), we observed the development of spontaneous Ca^{2+} releases that propagated as well-organized, cell-wide waves that spread rapidly throughout the cell (Figure 3A). The propagation velocity of waves in WT myocytes was uniform and averaged 127±7 μm/s (n=7). This behavior was at variance with that observed in CASQ2 mutant cells. In R33Q myocytes, multiple SCaEs failed to generate cell-wide propagating waves (n=12; Figure 3A, R33Q cells 1 and 2); rather they broke down into small localized Ca^{2+} release events before terminating. Propagation velocity was nonuniform and significantly slower than that of WT (51±8 μm/s; n=8; $P<0.01$). This observation was confirmed in saponin-permeabilized myocytes (Figure 3B). Once again, only WT myocytes developed spontaneous cell-wide Ca^{2+} waves (Figure 3B), whereas R33Q cells presented with chaotic, fragmented waves and wavelets (Figure 3B). We confirmed the presence of SCaEs (occurring between field-stimulated events) in the line-scan experiments (Figure 3A, R33Q cells 1 and 2). The occurrence of the early, multiple spontaneous Ca^{2+} rerelease events slowed the global Ca^{2+} transient decay, as shown in the Online Figure II.

To further characterize Ca^{2+} dynamics in R33Q cells, we investigated spatial and temporal characteristics of local SCaEs in intact myocytesusing 2D confocal microscopy. In the presence of Iso, SCaEs were infrequently seen in WT myocytes, but whenever they occurred, they rapidly propagated throughout the cell to form an organized cell-wide wave (Online Figure IIIA, WT). Local SCaEs followed each other from site to site during this propagation (Figure IIIB, WT). In contrast, SCaEs were of multiple origins in R33Q myocytes (Online Figure IIIA, R33Q cells 1 and 2); they spread slowly and failed to propagate within the entire cell (Online Figure IIIB, R33Q cell 1). Waves broke down into several wavelets (fragmented waves) before stopping (Online Figure IIIB, R33Q cell 2). Notably, global SCaEs profiles differ between WT and R33Q cells (compare global SCaEs [black lines] in Online Figure IIIB).

We tested different hypotheses to unveil the cause of fragmentation of the spontaneous Ca^{2+} waves. We initially

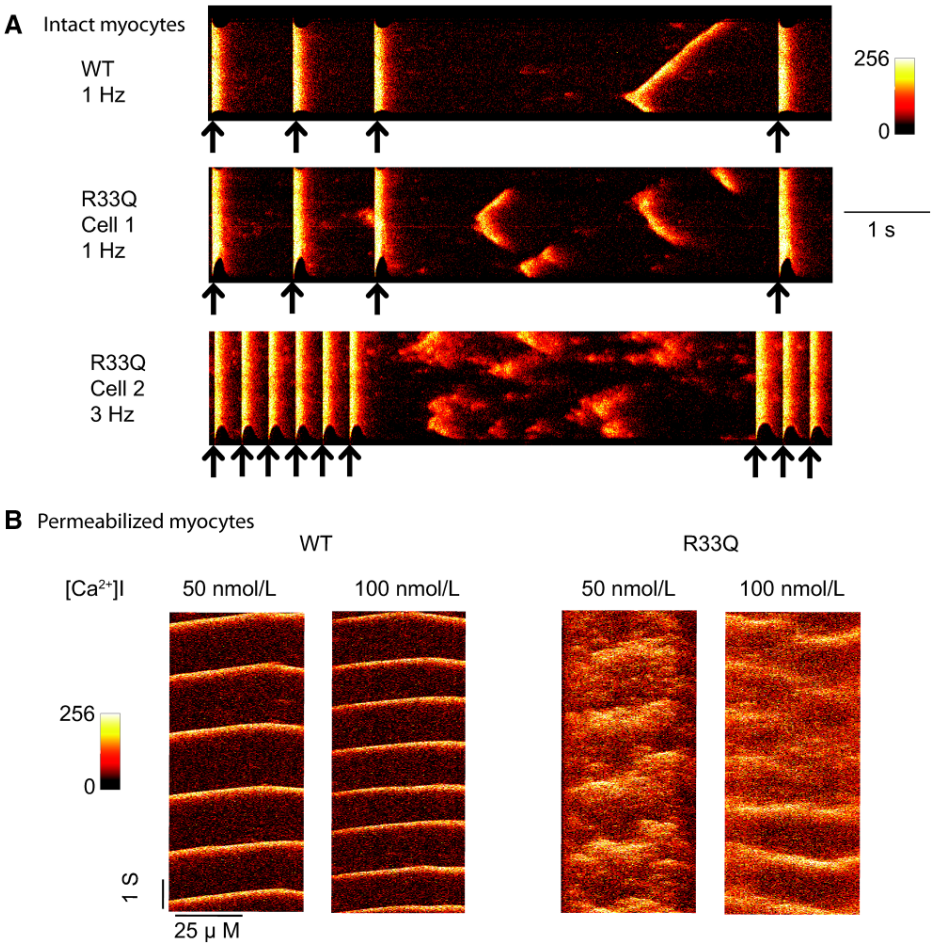

Figure 3. A, Representative confocal line-scan images show spontaneous Ca^{2+} release events (SCaEs) in wild-type (WT) and R33Q cells in the presence of isoproterenol (Iso). Black arrows indicate field stimulations. SCaEs in WT myocytes were usually due to a cell-wide wave that was initiated at 1 site. SCaEs in R33Q cells varied. Often, fragmented spontaneous Ca^{2+} waves occurred and slowly propagated (cells 1 and 2), and wavelets and Ca^{2+} sparks occurred before Ca^{2+} transients resume the diastolic level. B, Representative confocal line-scan images show spontaneous Ca^{2+} events in permeabilized WT and R33Q myocytes (EGTA, 0.05 mmol/L). Under this condition, WT myocytes exhibited regular spontaneous Ca^{2+} cell-wide waves; increasing $[Ca]^{2+}_i$ increased the frequency of spontaneous Ca^{2+} cell-wide waves. On the contrary, R33Q cells did not show cell-wide waves but rather presented with chaotic and fragmented events and wavelets.

speculated that depletion of SR Ca^{2+} in the adjacent region of spontaneous release could impair propagation. To test this hypothesis, we assessed whether spontaneous Ca^{2+} release occurred predominantly at the site in which failure to propagate occurred. But we were unable to establish a link between the site of spontaneous Ca^{2+} release and the region of fragmentation of waves; therefore, we dismissed this hypothesis. Next, we assessed whether impaired propagation of waves occurred in proximity of anatomic obstacles such as mitochondria; unfortunately, we were unable to find a relationship between the site of breakdown of Ca^{2+} waves and the presence of cellular structures. Thus, we dismissed this hypothesis.

We therefore went on to investigate whether fragmentation of spontaneous calcium waves in R33Q myocytes was because of structural and ultrastructural abnormalities.

Structural and Ultrastructural Features of R33Q Myocytes

Initially, di-4-ANEPPS: di-4-voltage sensitive aminonaphthylethenylpyridinium (ANEP) dyes staining was used to determine the distance between T tubules (TTs) in cells from WT and R33Q mice, and we observed that the average spatial distance between TTs in WT and R33Q myocytes was identical (1.83±0.01 μm in WT and 1.83±0.01 μm in R33Q; Online Figure IV). Subsequently, we investigated whether ultrastructural abnormalities were present and if they could justify the occurrence of aborted Ca^{2+} waves.

Previous electron microscopy observations[8] have shown that the width of the jSR terminal cisternae is on average increased in R33Q myocytes. This enlargement is likely caused by lack of the typical chain-like electron-dense polymer inside the jSR representing CASQ2 because it has been proposed that the association of CASQ2 to triadin and junctin holds the jSR lumen narrow.[16] Here, we extend our morphometric analyses and quantify the CRU frequency and length of contacts between jSR and TTs (ie, length of couplons) in tissues from WT and R33Q mice. We will refer to each of the structures depicted in Figure 4A through 4F as a CRU, whereas when jSR forms multiple contacts with the TT, as in Figure 4E and 4F, we will consider those contacts as different couplons. In WT (Figure 4A–4C), the jSR (labeled in yellow in Figure 4) is flat and forms usually long couplons with the TT (labeled in green in Figure 4). In R33Q cells, however, we found heterogeneity in the length of couplons, which appeared fragmented (Figure 4D and 4F). As shown in Online Figure V, the distribution of the length of couplons is shifted to the left in R33Q cells. Specifically, 50% of jSR/TT couplons are ≤100 nm in R33Q, whereas in WT 83% of couplons are >100 nm (median length of couplons was 193.5 nm in WT versus 100.3 nm in R33Q; $P<0.01$). We classified as fragmented those CRUs formed by 1 TT associated to ≥3 SR terminal cisternae (as in Figure 4F): this quantitative analysis indicates that in WT cardiac cells only 9% of couplons contained ≥3 SR terminal cisternae, whereas in R33Q, 28% of CRUs seems fragmented.

Although the overall number of CRUs and couplons did not vary significantly between WT and R33Q myocytes (Table 2, columns A and B), the average length of individual couplon between jSR and TT contacts was significantly shorter in R33Q myocytes than in WT myocytes (134±81 versus 213±128 nm; $P<0.001$; Table 2, column C). Assuming that (1) each couplon has an approximately round shape and (2) the electron microscopy sections cut a random chord of this circle (see Methods in Online Data Supplement for more details), the average area of contacts between jSR and TT is decreased by ≈60% in R33Q myocytes (Table 2, column D). Because the contact between jSR and TTs contains RyR2, a reduction in the area of contacts would imply less RyR2 in each couplon; therefore, it may at least partially account for impaired propagation of Ca^{2+} waves via Ca^{2+}-induced Ca^{2+} release (CICR). Considering that the approximate size of RyR-feet is ≈29×29 nm, the estimated number of RyR2-feet that would fit in such an area is significantly decreased in R33Q cells (n=27 R33Q; n=68 WT; Table 2, column E).

In addition to the number of RyRs, mathematical modeling studies[17] strongly support the idea that the jSR volume would be an important factor that could interfere with reduce the total amount of Ca^{2+} released by CRUs during excitation-contraction coupling. We measured the relative fiber volume occupied by jSR in both WT and R33Q cells (Table 2, column F) and verified that jSR volume is reduced by ≈30% ($P<0.01$) in R33Q versus WT (0.33±0.03 versus 0.23±0.02, respectively). We propose that in R33Q cells small sparks act in synergy with the reduction in length of couplons and jSR volume to impair activation of adjacent CRUs, reducing the ability of waves to propagate across the cells.[18,19]

Rescue of Structural Abnormalities and Impaired Propagation of Spontaneous Calcium Waves

To further establish the link between structural abnormalities and the fragmented propagation of spontaneous Ca^{2+} waves, we used an AAV9 vector to deliver WT *CASQ2* in vivo to R33Q hearts and studied the myocytes. We previously demonstrated that this protocol is able to achieve CASQ2 infection in 50% of cardiac myocytes and to significantly increase the levels of WT CASQ2.[11] We also reported that after *CASQ2*-AAV9 infection, afterdepolarizations disappeared and arrhythmias were no longer observed after adrenergic stimulation. Here, we investigated whether viral gene transfer of CASQ2 would be able to revert the impairment in Ca^{2+} wave propagation in saponin-permeabilized R33Q AAV9-treated myocytes at various cytoplasmic $[Ca^{2+}]_i$. First, we kept the cells in an internal solution containing 50 or 100 nmol/L free $[Ca]_i$ (0.05 mmol/L EGTA). Under these conditions, all WT myocytes generated periodic spontaneous Ca^{2+} cell-wide waves; increasing cytoplasmic $[Ca^{2+}]_i$ enhanced the frequency of spontaneous Ca^{2+} waves. Under similar conditions, none of untreated R33Q myocytes exhibited regular spontaneous Ca^{2+} waves; all permeabilized R33Q myocytes presented with fragmented waves. On the contrary, all R33Q myocytes infected with *CASQ2*-AAV9 exhibited periodic spontaneous Ca^{2+} cell-wide waves; there were no significant differences in frequency of spontaneous Ca^{2+} waves between WT and R33Q myocytes infected with *CASQ2*-AAV9 (n=12–18 from 3 mice; Figure 5A and 5B).

Interestingly, the structural abnormalities present in the R33Q cells also disappeared after infection with *CASQ2*-AAV9 (Figure 4G–4I).

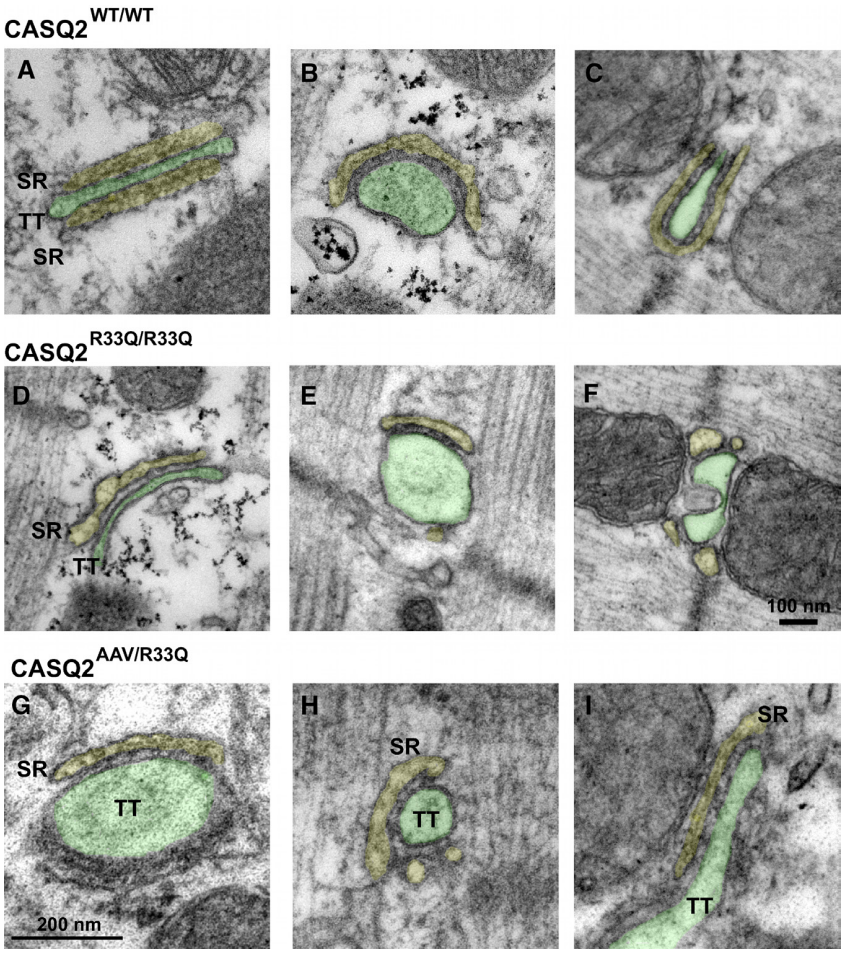

Figure 4. Ultrastructural analysis of junctional sarcoplasmic reticulum (jSR). Electron micrographs from thin sections of age-matched wild-type (WT), cardiac calsequestrin-2 (CASQ2 WT/WT), homozygous R33Q mutant mice (CASQ2 R33Q/R33Q), and CASQ2-R33Q mice infected with adeno-associated viral infected-CASQ2-R33Q (AAV-R33Q) A through C, In WT cells, the jSR (yellow) forms junctions (also called couplons) with the T tubule (TT, green), which are usually fairly extended. D through F, in R33Q cells, jSR/TT junctions can appear fairly normal in length (D), but other jSRs appear smaller (E) or fragmented (F). G through I, Effects of AVV-mediated infection of R33Q hearts with WT CASQ2: G, In WT myocytes, the jSR presents a narrow and □at pro□le surrounding the TT, with CASQ2 visible as chain-like electron-dense polymers, whereas in R33Q mutant myocytes (H), the jSR is fragmented, enlarged, and empty. CASQ2 re-expression by viral infection (I) rescues the chain-like polymer and restores the jSR narrow pro□le in AAV-R33Q cells (n=3 mice per group).

Afterdepolarizations in R33Q Myocytes

We recorded action potentials in WT and in R33Q myocytes in the presence of Iso and quantified the occurrence of afterdepolarizations and triggered activity (Online Table I). R33Q cells were more prone to the development of DADs, EADs, and triggered activity as compared with WT cells (Figures 6 and 7). Interestingly both types of afterpotentials occurred over the broad range of pacing frequencies only in R33Q cells (Figure 7).

EADs occurred at depolarized potentials (the takeoff potential recorded from 27 R33Q cardiac cells showed a mean value of −42.8±1.8 mV), leading to prolongation and distortion of the shape of the action potential (Figure 7). Afterdepolarizations also occurred during the diastolic phase between paced beats, creating instability of the diastolic potential (Figure 7). Poincaré plots[20] showed an increase of short-term variability in diastolic membrane potential and in duration of action potential duration at 90% (APD_{90}) in R33Q cells compared with WT cells (Figure 6A and 6B). The presence of small-amplitude, nontriggering afterdepolarizations (see high-magnification insets in Figure 7) is consistent with the presence of nonpropagating Ca^{2+}waves that induce subthreshold voltage oscillations. The occurrence of irregular duration of APD_{90} and the presence of heterogeneity in the diastolic membrane potential identify a novel arrhythmogenic substrate in CPVT.

This was further confirmed by exposing R33Q myocytes that presented EADs and DADs to ryanodine (10 μmol/L).

Table 2. Ultrastructural Morphometry of CRUs

	A	B	C*	D*	E*	F*
	No. of CRUs/20 μm²	No. of Couplons/20 μm²	Average Couplon Length, nm	Estimated Couplon Area, μm²	Estimated No. of RyR-Feet/Couplon	jSR\Volume/Total Vol, %
WT	2.2□1.5 (67)	2.42□1.74 (67)	213□128 (115)	0.057	68	0.33□0.03 (67)
R33Q	2.1□1.5 (77)	2.65□1.72 (77)	134□81 (122)	0.023	27	0.23□0.02 (77)

All data were collected from 3 hearts of R33Q and 3 hearts of WT mice and expressed as mean□SD. In parentheses are the numbers of cardiac cells analyzed (columns A, B, and F) and numbers of couplons analyzed (column C). CRU indicates Ca^{2+} release unit; jSR, junctional sarcoplasmic reticulum; RyR, ryanodine receptor-2; and WT, wild-type.

*P<0.001 vs WT.

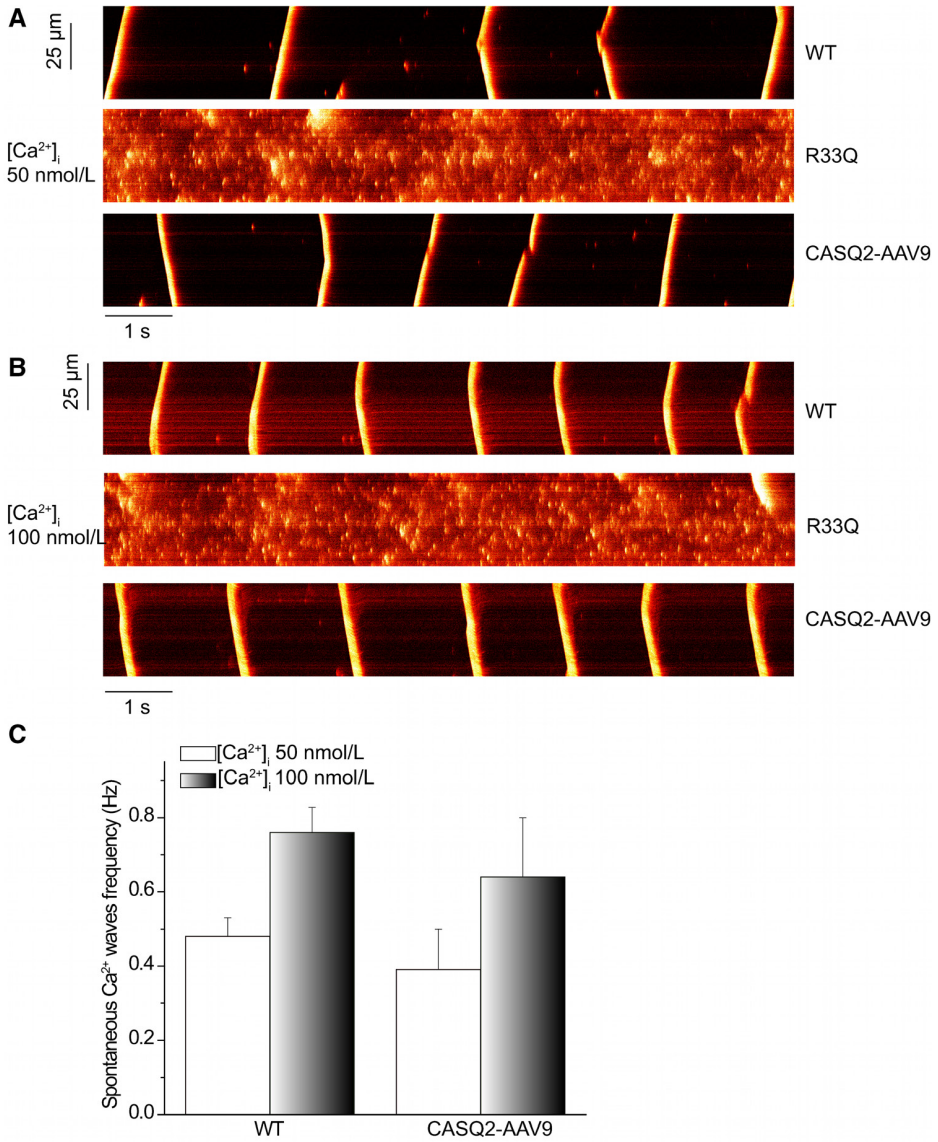

Figure 5. A and B, Representative confocal line-scan images show spontaneous Ca^{2+} events in permeabilized R33Q, wild-type (WT), and cardiac calsequestrin-2 (CASQ2)–AAV9 cells in the presence of $[Ca]^{2+}_i$ 50 and 100 nmol/L. R33Q cells did not show cell-wide waves but presented with chaotic, fragmented events and wavelets. WT and CASQ2-AAV9 myocytes exhibited regular spontaneous Ca^{2+} cell-wide waves; increasing $[Ca]^{2+}_i$ increased the frequency of Ca^{2+} cell-wide waves. C, There was no significant difference in Ca^{2+} wave frequency of WT and CASQ2-AAV9 myocytes. n=12 to 18 cells in each group.

Ryanodine abolished EADs and DADs in all 6 cells (Online Figure VI). This suggests that the abnormal Ca^{2+} releases underlie these arrhythmogenic voltage changes.

Discussion

The aim of the present study was to characterize the behavior of paced Ca^{2+} transients and adrenergically mediated spontaneous Ca^{2+} sparks and waves in myocytes derived from WT and CASQ2-R33Q knock-in mice. Unexpectedly, we observed that the behavior of SCaEs in R33Q myocytes is markedly different from that observed in myocytes derived from our $RyR2^{R4496C+/-}$ CPVT mouse model[21] and from the data obtained in published models of recessive CPVT.[13,22] R33Q myocytes showed an abnormally short coupling of SCaEs to the previous paced activation and a remarkable fragmentation of the SCaEs. Cells isolated from the heart of $RyR2^{R4496C+/-}$ mice seldom develop SCaEs between paced beats and present with well-organized Ca^{2+} release events that propagate quickly to form a typical cell-wide wave.[2,21,23] In R33Q myocytes, the occurrence of short-coupled SCaEs is mirrored by the abbreviated spark-to-spark coupling interval (Figure 2B) that is suggestive of an acceleration in RyR2 recovery from refractoriness and faster refilling of the SR.[24,25] Recent data have shown that the absence of CASQ2 accelerates RyR2 refractoriness, which is determined predominantly by Ca^{2+} refilling in jSR,[15] a process that is influenced by CASQ2 Ca^{2+}-buffering capacity.[14,26] In Limitations in the Online Data Supplement, we highlight technical limitations in the resolution of spark activity that might affect the measurement of SR refractoriness.

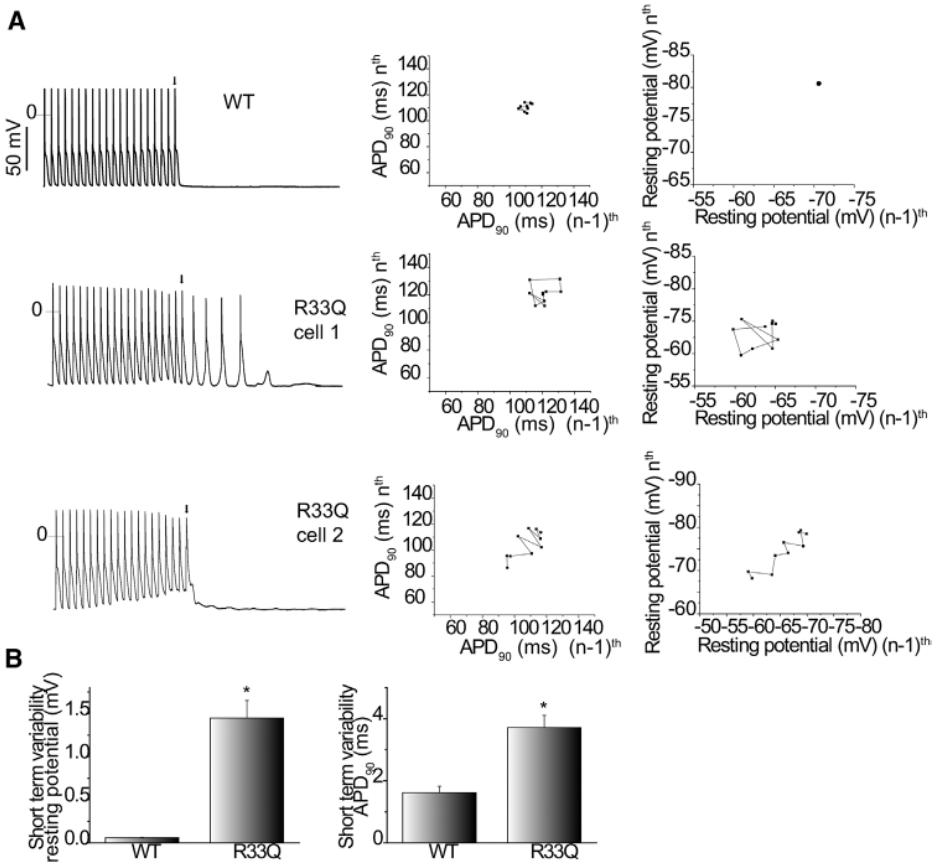

Figure 6. A, Left, Action potential recordings in the presence of isoproterenol (30 nmol/L) at 5-Hz pacing. Arrows indicate the last pacing. Wild-type (WT) cell showed no delayed afterdepolarizations (DADs); R33Q cell 1 exhibited typical triggered activities, and R33Q cell 2 presented membrane voltage oscillation after the cessation of field stimulation. Middle and Right, Poincaré plots of APD_{90} and resting potential of right cells, respectively (the last 10 sequential action potential). Resting potential was corrected by liquid junction potential. B, Short-term variability for APD_{90} and resting potential is larger in R33Q cells than in WT cells (*$P<0.01$ vs WT; n=12–15 cells for each group).

To understand the cause of fragmentation of SCaEs, we tested different hypotheses and ruled out several. We then hypothesized that the impaired propagation of Ca^{2+} waves could be related to a disarray of the couplons and performed morphological studies to test this hypothesis. Electron microscopy evaluation in our model revealed smaller jSR contact length (Table 2, column C) that is predicted to fit a smaller array of RyR2s (Table 2, column E). We measured the relative fiber volume occupied by the jSR and verified that this is reduced in R33Q myocytes. The combined effect of these structural changes is expected to be a reduction in the amount of Ca^{2+} released during CICR and therefore is in agreement with our measured Ca^{2+} spark properties in the R33Q myocytes. Because the propagation of spontaneous Ca^{2+} waves relies on RyR2 activation by neighboring RyR2 via CICR,[27,28] we suggest that the smaller amount of local SR Ca^{2+} release (a combination of smaller RyR2 arrays and reduced jSR volume), evidenced by the smaller spark mass in R33Q cells (Table 1), would simply not be able to raise local $[Ca]^{2+}_i$ at the next CRU to the level required for its activation. Thus, this would reduce greatly the safety factor for wave propagation via CICR in R33Q cells. Our electron microscopy study revealed the heterogeneity in the length of couplons in R33Q myocytes, suggesting that in R33Q myocytes there are only 40% of couplons with lengths similar to those observed in WT (Online Figure V). Thus, the heterogeneity of couplons may account for the heterogeneity observed in R33Q wave propagation: in fact, some waves do not propagate, whereas others travel small distances at a reduced propagation velocity before stopping.

The evidence that exogenous administration of cDNA of WT *CASQ2* by systemic AAV injection to the R33Q mice is able to rescue the ultrastructural abnormality and restore normal calcium wave propagation in the R33Q mutant, strongly suggests that remodeled CRUs in R33Q myocytes are likely determinants of the fragmented Ca^{2+} waves.

Overall our data show that the consequences of R33Q are multiple and that their interplay creates a complex substrate. For example, the reduction of CASQ2 protein that occurs in the presence of the R33Q mutant impairs the Ca^{2+}-buffering capacity of R33Q myocytes and causes rapid Ca^{2+} diffusion in SR. This behavior hampers the accumulation of Ca^{2+} in the luminal side of RyR2;[29,30] thus altering the luminal Ca^{2+}-dependent component of propagation of spontaneous Ca^{2+} waves.

Interestingly, we observed slower global Ca^{2+} transient decay in R33Q myocytes compared with WT. The reasons for the delayed Ca^{2+} reuptake can be attributed to the reduced Ca^{2+}-buffering capacity in SR of R33Q myocytes. The reuptake rate is limited by intra-SR free $[Ca]^{2+}_i$ by back-inhibition on the Ca^{2+} pump as previously described in CASQ1 knockout myocytes.[31,32] In addition, Guo et al[33] more recently reported that spontaneous Ca^{2+} releases during twitch $[Ca]^{2+}_i$ decline slow global $[Ca]^{2+}_i$ decline. We show that this also occurs in R33Q myocytes as evidenced by the early phase of Ca^{2+} rereleases observed during paced beats (Online Figure II). This is consistent with the shortened refractoriness of the RyR2 channel.

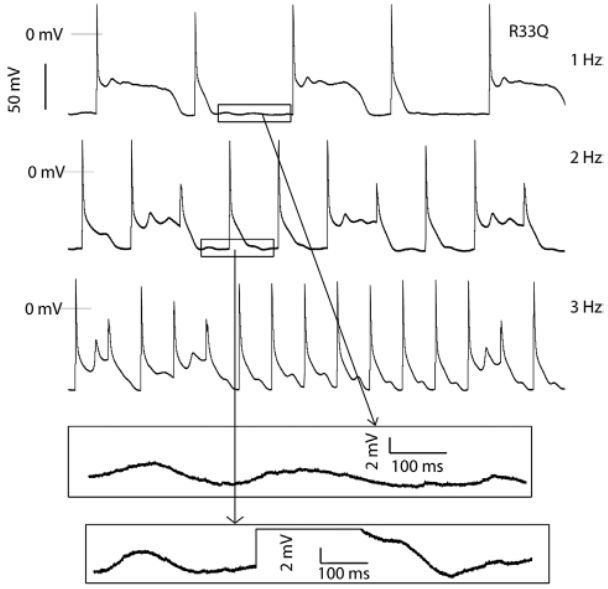

Figure 7. Action potentials recordings in a R33Q mouse in the presence of isoproterenol (30 nmol/L) at 1- to 3-Hz pacing. Resting potential was corrected by liquid junction potential. Early afterdepolarizations occurred at lower pacing frequency; diverse patterns of action potential were shown in all pacing frequencies. Bottom, The enlarged membrane oscillations occurring between stimulated beats.

Arrhythmogenesis in R33Q Hearts

The characterization of the electrophysiological properties of the R33Q myocytes revealed that the electric substrate of R33Q cells is rather unique and differs from that previously reported in other CPVT models. We show (Figure 1) that during exposure to Iso, R33Q cardiac cells present SCaEs with variable coupling intervals to the preceding paced beat that promote development of afterpotentials. These occur not only during phase 4 of the action potential (DADs) but also during phase 2 or 3 of the action potential (EADs). Furthermore, both types of afterdepolarizations are promptly abolished with exposure to ryanodine and thus are caused by SR calcium release (Online Figure VI). Action potential recordings in R33Q myocytes suggest that the chaotic occurrence of afterpotentials at various coupling intervals perturbs the stability of the action potential and of the diastolic membrane potential (Figures 6 and 7). Both characteristics are likely to increase the propensity for development of sustained arrhythmic events and to provide a novel substrate for arrhythmias in CPVT.[34]

Conclusions

We demonstrated that arrhythmogenesis in CASQ2-R33Q mice is the consequence of a cascade of events that generate a complex arrhythmogenic substrate.

The 2 pivotal determinants of electric instability in R33Q myocytes are the changes in CRU architecture (reduction of couplon length and jSR volume) and the accelerated Ca^{2+} rereleases from the SR. The former reduces Ca^{2+}spark mass, forcing less $[Ca]^{2+}_i$ increase at neighboring CRUs during CICR, leading to impaired propagation of Ca^{2+} waves and thus development of subthreshold voltage oscillations that destabilize diastolic membrane potential. The latter suggests that the loss of CASQ2 presents with reduced refractoriness of RyR2, promoting the occurrences of multiple short-coupled rereleases and thus the development of afterdepolarizations with variable coupling intervals immediately after peak transient. This then leads to the heterogeneity of action potential duration and possible occurrence of EADs. This setting is entirely different and more complex than the one present in mice models of the dominant form of CPVT and may account for the higher lethality of CASQ2-related CPVT.[1,30]

Disclosures

This work was supported by Telethon grants GGP11141 and GGP06007 (to S.G. Priori) and GGP08153 (to F. Protasi), Fondazione CARIPLO pr.2008.2275; by Fondation Leducq Award to the Alliance for Calmodulin Kinase Signaling in Heart Disease (08CVD01; to S.G. Priori); by the FondazioneVeronesi Award on inherited arrhythmogenic diseases (to S.G. Priori); and by National Institutes of Health grant HL 066140 (to P.A. Boyden). The other authors have no conflict to report.

References

1. Liu N, Ruan Y, Priori SG. Catecholaminergic polymorphic ventricular tachycardia. *Prog Cardiovasc Dis*. 2008;51:23–30.
2. Liu N, Colombi B, Memmi M, Zissimopoulos S, Rizzi N, Negri S, Imbriani M, Napolitano C, Lai FA, Priori SG. Arrhythmogenesis in catecholaminergic polymorphic ventricular tachycardia: insights from a RyR2 R4496C knock-in mouse model. *Circ Res*. 2006;99:292–298.
3. Kannankeril PJ, Mitchell BM, Goonasekera SA, et al. Mice with the R176Q cardiac ryanodine receptor mutation exhibit catecholamine-induced ventricular tachycardia and cardiomyopathy. *Proc Natl Acad Sci U S A*. 2006;103:12179–12184.
4. Uchinoumi H, Yano M, Suetomi T, Ono M, Xu X, Tateishi H, Oda T, Okuda S, Doi M, Kobayashi S, Yamamoto T, Ikeda Y, Ohkusa T, Ikemoto N, Matsuzaki M. Catecholaminergic polymorphic ventricular tachycardia is caused by mutation-linked defective conformational regulation of the ryanodine receptor. *Circ Res*. 2010;106:1413–1424.
5. Lehnart SE, Mongillo M, Bellinger A, Lindegger N, Chen BX, Hsueh W, Reiken S, Wronska A, Drew LJ, Ward CW, Lederer WJ, Kass RS, Morley G, Marks AR. Leaky Ca2+ release channel/ryanodine receptor 2 causes seizures and sudden cardiac death in mice. *J Clin Invest*. 2008;118:2230–2245.
6. Liu N, Rizzi N, Boveri L, Priori SG. Ryanodine receptor and calsequestrin in arrhythmogenesis: what we have learnt from genetic diseases and transgenic mice. *J Mol Cell Cardiol*. 2009;46:149–159.
7. Song L, Alcalai R, Arad M, Wolf CM, Toka O, Conner DA, Berul CI, Eldar M, Seidman CE, Seidman JG. Calsequestrin 2 (CASQ2) mutations increase expression of calreticulin and ryanodine receptors, causing catecholaminergic polymorphic ventricular tachycardia. *J Clin Invest*. 2007;117:1814–1823.
8. Rizzi N, Liu N, Napolitano C, et al. Unexpected structural and functional consequences of the R33Q homozygous mutation in cardiac calsequestrin: a complex arrhythmogenic cascade in a knock in mouse model. *Circ Res*. 2008;103:298–306.
9. Knollmann BC, Chopra N, Hlaing T, Akin B, Yang T, Ettensohn K, Knollmann BE, Horton KD, Weissman NJ, Holinstat I, Zhang W, Roden DM, Jones LR, Franzini-Armstrong C, Pfeifer K. Casq2 deletion causes sarcoplasmic reticulum volume increase, premature Ca2+ release, and catecholaminergic polymorphic ventricular tachycardia. *J Clin Invest*. 2006;116:2510–2520.
10. Picht E, Zima AV, Blatter LA, Bers DM. SparkMaster: automated calcium spark analysis with ImageJ. *Am J Physiol Cell Physiol*. 2007;293:C1073–C1081.
11. Denegri M, Avelino-Cruz JE, Boncompagni S, De Simone SA, Auricchio A, Villani L, Volpe P, Protasi F, Napolitano C, Priori SG. Viral gene transfer rescues arrhythmogenic phenotype and ultrastructural abnormalities in adult calsequestrin-null mice with inherited arrhythmias. *Circ Res*. 2012;110:663–668.
12. Mobley BA, Eisenberg BR. Sizes of components in frog skeletal muscle measured by methods of stereology. *J Gen Physiol*. 1975;66:31–45.
13. Kalyanasundaram A, Viatchenko-Karpinski S, Belevych AE, Lacombe VA, Hwang HS, Knollmann BC, Gyorke S, Periasamy M. Functional consequences of stably expressing a mutant calsequestrin (CASQ2D307H)

in the CASQ2 null background. *Am J Physiol Heart Circ Physiol*. 2012;302:H253–H261.
14. Ramay HR, Liu OZ, Sobie EA. Recovery of cardiac calcium release is controlled by sarcoplasmic reticulum refilling and ryanodine receptor sensitivity. *Cardiovasc Res*. 2011;91:598–605.
15. Kornyeyev D, Petrosky AD, Zepeda B, Ferreiro M, Knollmann B, Escobar AL. Calsequestrin 2 deletion shortens the refractoriness of Ca^{2+} release and reduces rate-dependent Ca^{2+}-alternans in intact mouse hearts. *J Mol Cell Cardiol*. 2012;52:21–31.
16. Tijskens P, Jones LR, Franzini-Armstrong C. Junctin and calsequestrin overexpression in cardiac muscle: the role of junctin and the synthetic and delivery pathways for the two proteins. *J Mol Cell Cardiol*. 2003;35:961–974.
17. Lee YS, Liu OZ, Hwang HS, Knollmann BC, Sobie EA. Parameter sensitivity analysis of stochastic models provides insights into cardiac calcium sparks. *Biophys J*. 2013;104:1142–1150.
18. Sobie EA, Guatimosim S, Gómez-Viquez L, Song LS, Hartmann H, Saleet Jafri M, Lederer WJ. The Ca 2+ leak paradox and rogue ryanodine receptors: SR Ca 2+ efflux theory and practice. *Prog Biophys Mol Biol*. 2006;90:172–185.
19. Hüser J, Bers DM, Blatter LA. Subcellular properties of [Ca2+]i transients in phospholamban-deficient mouse ventricular cells. *Am J Physiol*. 1998;274:H1800–H1811.
20. Thomsen MB, Verduyn SC, Stengl M, Beekman JD, de Pater G, van Opstal J, Volders PG, Vos MA. Increased short-term variability of repolarization predicts d-sotalol-induced torsades de pointes in dogs. *Circulation*. 2004;110:2453–2459.
21. Liu N, Denegri M, Ruan Y, Avelino-Cruz JE, Perissi A, Negri S, Napolitano C, Coetzee WA, Boyden PA, Priori SG. Short communication: flecainide exerts an antiarrhythmic effect in a mouse model of catecholaminergic polymorphic ventricular tachycardia by increasing the threshold for triggered activity. *Circ Res*. 2011;109:291–295.
22. Stevens SC, Terentyev D, Kalyanasundaram A, Periasamy M, Györke S. Intra-sarcoplasmic reticulum Ca2+ oscillations are driven by dynamic regulation of ryanodine receptor function by luminal Ca2+ in cardiomyocytes. *J Physiol*. 2009;587:4863–4872.
23. Liu N, Ruan Y, Denegri M, Bachetti T, Li Y, Colombi B, Napolitano C, Coetzee WA, Priori SG. Calmodulin kinase II inhibition prevents arrhythmias in RyR2(R4496C+/-) mice with catecholaminergic polymorphic ventricular tachycardia. *J Mol Cell Cardiol*. 2011;50:214–222.
24. Picht E, Zima AV, Shannon TR, Duncan AM, Blatter LA, Bers DM. Dynamic calcium movement inside cardiac sarcoplasmic reticulum during release. *Circ Res*. 2011;108:847–856.
25. Terentyev D, Kubalova Z, Valle G, Nori A, Vedamoorthyrao S, Terentyeva R, Viatchenko-Karpinski S, Bers DM, Williams SC, Volpe P, Gyorke S. Modulation of SR Ca release by luminal Ca and calsequestrin in cardiac myocytes: effects of CASQ2 mutations linked to sudden cardiac death. *Biophys J*. 2008;95:2037–2048.
26. Terentyev D, Viatchenko-Karpinski S, Györke I, Volpe P, Williams SC, Györke S. Calsequestrin determines the functional size and stability of cardiac intracellular calcium stores: mechanism for hereditary arrhythmia. *Proc Natl Acad Sci U S A*. 2003;100:11759–11764.
27. Cheng H, Lederer MR, Lederer WJ, Cannell MB. Calcium sparks and [Ca2+]i waves in cardiac myocytes. *Am J Physiol*. 1996;270:C148–C159.
28. Ter Keurs HE, Boyden PA. Calcium and arrhythmogenesis. *Physiol Rev*. 2007;87:457–506.
29. Ramay HR, Jafri MS, Lederer WJ, Sobie EA. Predicting local SR Ca(2+) dynamics during Ca(2+) wave propagation in ventricular myocytes. *Biophys J*. 2010;98:2515–2523.
30. Swietach P, Spitzer KW, Vaughan-Jones RD. Modeling calcium waves in cardiac myocytes: importance of calcium diffusion. *Front Biosci*. 2010;15:661–680.
31. Fryer MW, Stephenson DG. Total and sarcoplasmic reticulum calcium contents of skinned fibres from rat skeletal muscle. *J Physiol*. 1996;493(Pt 2):357–370.
32. Paolini C, Quarta M, Nori A, Boncompagni S, Canato M, Volpe P, Allen PD, Reggiani C, Protasi F. Reorganized stores and impaired calcium handling in skeletal muscle of mice lacking calsequestrin-1. *J Physiol*. 2007;583:767–784.
33. Guo T, Zhang T, Ginsburg KS, Mishra S, Brown JH, Bers DM. CaMKIIδC slows [Ca]i decline in cardiac myocytes by promoting Ca sparks. *Biophys J*. 2012;102:2461–2470.
34. Weiss JN, Qu Z, Chen PS, Lin SF, Karagueuzian HS, Hayashi H, Garfinkel A, Karma A. The dynamics of cardiac fibrillation. *Circulation*. 2005;112:1232–1240.

Novelty and Significance

What Is Known?

- Homozygous mutations in the cardiac calsequestrin-2 (CASQ2) gene cause recessive catecholaminergic polymorphic ventricular tachycardia and predispose to cardiac arrest.
- Transgenic mice carriers of CASQ2 mutations show spontaneous calcium release events in response to adrenergic stimulation that generate delayed afterdepolarizations, leading to life-threatening ventricular arrhythmias.
- These mice also have decreased levels of calsequestrin and the sister proteins triadin and junctin, as well as dilatation of the junctional sarcoplasmic reticulum (jSR).

What New Information Does This Article Contribute?

- Arrhythmogenesis associated with homozygous CASQ2 mice is more complex than previously thought.
- Transgenic mice carriers of the homozygous R33Q CASQ2 mutation show disruption of the calcium release apparatus, fragmentation of jSR, and reduction of jSR volume.
- These ultrastructural abnormalities impair the propagation of spontaneous calcium waves. The reduced volume of jSR leads to smaller calcium sparks with a short coupling interval, suggesting abnormally reduced refractoriness of the ryanodine receptor.
- At variance with current understanding, the arrhythmogenic mechanisms in CASQ2-R33Q include both delayed and early afterdepolarizations.

Until now, the ultrastructural abnormalities observed in CASQ2-deficient mice were not associated with functional abnormalities. In this study, we demonstrate that the presence of an abnormal architecture of the jSR leads to smaller calcium sparks tightly coupled to each other, suggesting that ryanodine receptor-2 refractoriness might also be impaired, possibly as a consequence of reduced levels of CASQ2. Spontaneous calcium release events were also profoundly altered in R33Q myocytes: they were of multiple origins, spread slowly, and failed to propagate within the entire cell. Often, these waves broke down into fragmented waves before stopping. These abnormal spontaneous calcium release events generated early and delayed afterdepolarizations, as well as small-amplitude, nontriggering afterdepolarizations that are the electric counterpart of nonpropagating Ca^{2+} waves that induce subthreshold voltage oscillations. By reintroducing calsequestrin via viral gene therapy, we were able to revert structural abnormalities and to prevent arrhythmogenesis. Overall, the findings of this study redefine recessive catecholaminergic polymorphic ventricular tachycardia as a disease caused by structural disruption of jSR architecture caused by lack of calsequestrin, suggesting that recessive catecholaminergic polymorphic ventricular tachycardia can be considered an ultrastructural cardiomyopathy. Gene therapy to restore levels of calsequestrin may be a therapeutic approach for patients with recessive catecholaminergic polymorphic ventricular tachycardia.

Abnormal propagation of calcium waves and ultrastructural remodeling in recessive catecholaminergic polymorphic ventricular tachycardia

Methods

Isolation of adult mice ventricular myocytes

Ventricular myocytes were isolated using an established enzymatic digestion protocol[1]. Within 6 hours after isolation, laminin-coated dishes containing isolated ventricular myocytes were mounted on the stage of an inverted microscope. The myocytes were bathed with the solution containing (mmol/L): 140 NaCl, 4 KCl, 2 $CaCl_2$, 1 $MgCl_2$, 10 HEPES and 5 glucose, pH adjusted to 7.4 with NaOH.

Ca^{2+} measurements

Isolated ventricular myocytes were incubated with 2.5 μM Fluo-4 AM (Invitrogen Inc., Eugene, OR) for 10 minutes at room temperature and washed twice with Tyrode's solution, then equilibrated in fresh Tyrodes solution containing 250 μM probenecid for 20 min to allow deesterification of the dye before recording. Fluorescent signals were acquired using a 40X UVF objective (numerical aperture 1.0, Nikon), and single excitation wavelength microfluorimetry was performed using a PMT system (IonOptix Corp., Milton, MA). Cells were field-stimulated (voltage 25% above threshold) to achieve steady-state at least 20 beats. Spontaneous Ca^{2+} release events (SCaEs) were defined as unstimulated increases in intracellular Ca^{2+} and were quantified during the 5 second unpaced interval following the train pacing. SR Ca^{2+} load was measured as the amplitude of the 10 mmol/L caffeine-induced Ca^{2+} transient.

In a set of experiment, spatial and temporal characteristics of local spontaneous Ca^{2+} events were measured by using 2D spinning disk (Nipkow) confocal microscopy. The intensity of the Ca^{2+}-related fluorescence was captured from the illumination field and light intensity was collected using a fast charge-coupled device camera (ORCA-ER C4742-95, Hamamatsu Photonics KK, Japan). The system was attached to the video port of an inverted microscope equipped with 60× oil objective lens. Conduction velocity of Ca^{2+} waves was calculated as the distance traveled in a certain amount of time. In WT myocytes, Ca^{2+} wave propagated at nearly a constant velocity. Ca^{2+} wave propagation velocity in R33Q myocytes was non uniform, so in R33Q myocytes, we chose Ca^{2+} waves propagation more than 25 μm for analysis and calculated the velocity of the initial 15 μm wave propagation.

For Ca^{2+} spark measurement, line-scan mode in confocal microscopy (Leica SP5) was used (400Hz) with a 64 oil-immersion objection. Spontaneous Ca^{2+} sparks intact myocytes were obtained in quiescent cells. We also investigated the Ca^{2+} handling in permeabilized myocytes. Cardiac myocytes were permeabilized by incubating with 0.01% saponin for 1.5 min and placed in a solution containing (in mmol/L): 120 potassium aspartate, 3 MgATP, 10 phosphocreatine, 5 U/ml creatine phosphokinase, 10 reduced glutathione, 0.5 or 0.05 EGTA, 1 free [Mg^{2+}], 4% dextran (relative molecular mass: 40 000), 0.05 K_4Fluo-4 and 10 Hepes. Free $[Ca^{2+}]_i$ was calculated by WINMAXC32 2.51. The dye was excited at 488 nm and emission was collected at >510 nm. Image analyses were performed with spark master in Imaging J software[2]. Spark mass was calculated as amplitude × 1.206 × FWHM.[3]

Electrophysiological recordings in isolated ventricular myocytes

Transmembrane potentials were recorded in whole-cell mode using a multiClamp 700B amplifier (Axon Instruments). The pipette solutions contained (in mmol/L): 120 potassium aspartate, 20 KCl, 1 $MgCl_2$, 4 Na_2ATP, 0.1 GTP, 10 HEPES, 10 glucose, pH 7.2, with NaOH. All signals were low-pass filtered at 5 kHz (Digidata 1440A, Axon Instruments) and analyzed using pCLAMP version 10.2 software (Axon Instruments). Only quiescent, Ca^{2+}-tolerant, rod-shaped cells with clear cross striations were used for electrophysiological recordings. Myocytes were electrically stimulated by intracellular current injection

through patch electrodes using depolarizing pulses. To induce afterdepolarizations and triggered activity we superfused the cells with Isoproterenol (30 nmol/L) for 10 minutes. Myocytes were electrically stimulated with pacing protocols at 1-3 Hz. To evaluate whether we could abolish afterdepolarizations with Ryanodine, we added the drug to the perfusion solution at the concentration of 10 μmol/L. Delayed afterdepolarizations (DADs) were defined as phase 4 positive (depolarizing) deflections of the membrane potential. Early afterdepolarizations (EADs) were defined as positive (depolarizing) oscillations occurring during phase 2 or 3 of action potential. Triggered activity was defined as an unstimulated action potential developing from a DAD or EAD. The liquid junction potential between pipette and bath solution was calculated with pCLAMP software and corrected after experiments.

The Poincaré analysis plots each value against the previous value and the orthogonal distance from these points to the diagonal is a measure of short-term variability. The mean orthogonal distance from the diagonal to the points on the Poincaré plot of diastolic membrane potential and APD90 were used as a measure of beat-to-beat variability or short term variability. The mean orthogonal distance was calculated according to the formula[3]: short term variability = $\Sigma | Dn+1 - Dn | / [N\text{tot} \times (2)1/2]$, where D represents diastolic membrane potential or APD_{90} . Poincaré analysis was performed on a subset of cells subjected to the last 10 stimulated beats.

Electron microscopy

The hearts were fixed by retrograde aortic perfusion. Small bundles of cells teased from the papillary muscles were then post-fixed in 2% OsO_4 in NaCaCo buffer for 2 hr and block-stained in saturated uranyl acetate. After dehydration, specimens were embedded in an epoxy resin (Epon 812). Ultrathin sections were cut in a Leica Ultracut R microtome (Leica Microsystem, Austria) using a Diatome diamond knife (DiatomeLtd. CH-2501 Biel, Switzerland) and double-stained with uranyl acetate and lead citrate. The Ultrastructural morphometry of CRUs were measured with Photoshop (Adobe Systems).

jSR volume calculation

The jSR volume was calculated by the well-established stereology point counting technique[4] in electron micrographs taken at 24,000 X, from cross-sections of papillary cardiomyocytes. In each fiber 2 or 3 pictures were taken in internal areas of the fibers, excluding the nuclei regions. The images were covered with an orthogonal arrays of dots at a spacing of 0.17 μm. The ratio of the dots' number falling over the jSR to the total number of dots covering the whole micrograph was used to calculate the percentage of fiber volume occupied by jSR.

Data Analysis

Data were expressed as mean±SEM. A Student t-test or a Mann-Whitney rank sum test was used to determine statistical significance between 2 groups. We used a 1-way ANOVA for multiple comparisons and Turkey post-hoc analysis between groups was used for pairwise comparison in ANOVA. Chi-square and Fisher's exact test were used as appropriate for non-parametric data. Differences with $p \leq 0.05$ were considered statistically significant.

LIMITATIONS

In our measures of sparks using line scan microscopy, we sought higher spatial and time resolution than that of our 2D microscopy studies. However, we were unable to discern activity at a submicron level to evaluate repetitive spark activity at the SAME junctional site. Therefore, our measured "SR

refractoriness" may be shorter than observed. On the other hand our EM studies focussed on the dyadic structures of WT and R33Q and "rescued" R33Q cells. Here we have spatial resolution of the static substrate but at this time are unable to query the nature of nonjunctional RyRs.

Online Table I
Occurrence of DADs, EADs and triggered activity in WT and R33Q myocytes in the presence of Iso (30 nmol/L)

	WT (n=18)	R33Q (n=19)
DADs	33%	89%*
EADs	0%	32%*
Triggered activity	0%	47%*

* $p<0.01$, vs WT

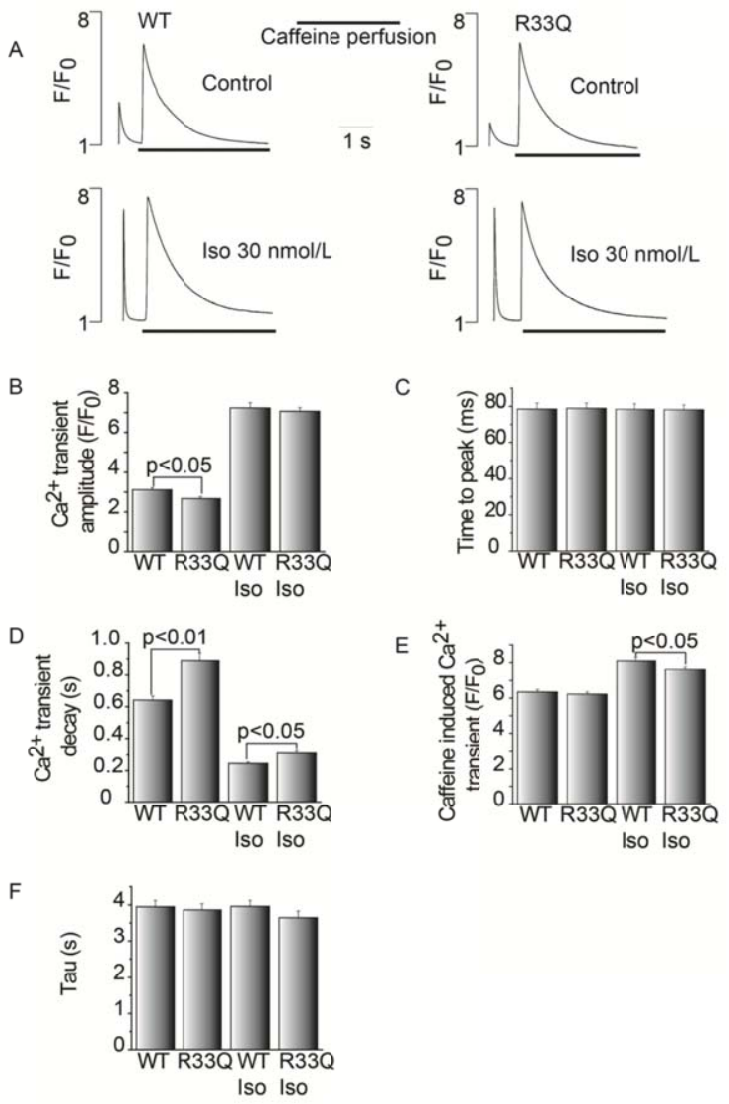

Online Figure I

Online Figure I

A, Original recordings of caffeine (10 mmol/L) induced Ca^{2+} transients in WT and R33Q cells after 0.2 Hz pacing. **B**, Average of Ca^{2+} transient amplitude (F/F_0) in WT and R33Q myocytes. R33Q cells showed reduced Ca^{2+} transient amplitude compared with WT, Iso abolished the differences in Ca^{2+} transient amplitude. **C**, Average of time to peak 90% of Ca^{2+} transient in WT and R33Q myocytes. **D**, Average of Ca^{2+} transient decay in WT and R33Q myocytes. R33Q myocytes showed slower Ca^{2+} transient decay compared with WT myocytes in the absence and the presence of Iso. **E**, Average of caffeine induced Ca^{2+} transient in WT and R33Q myocytes. R33Q cells showed reduced releasable Ca^{2+} compared with WT in the presence of Iso. **F**, Average of decay rate constant of caffeine induced Ca^{2+} transient showed identical sodium-calcium function in WT and R33Q myocytes. n=15-25 cells in each group.

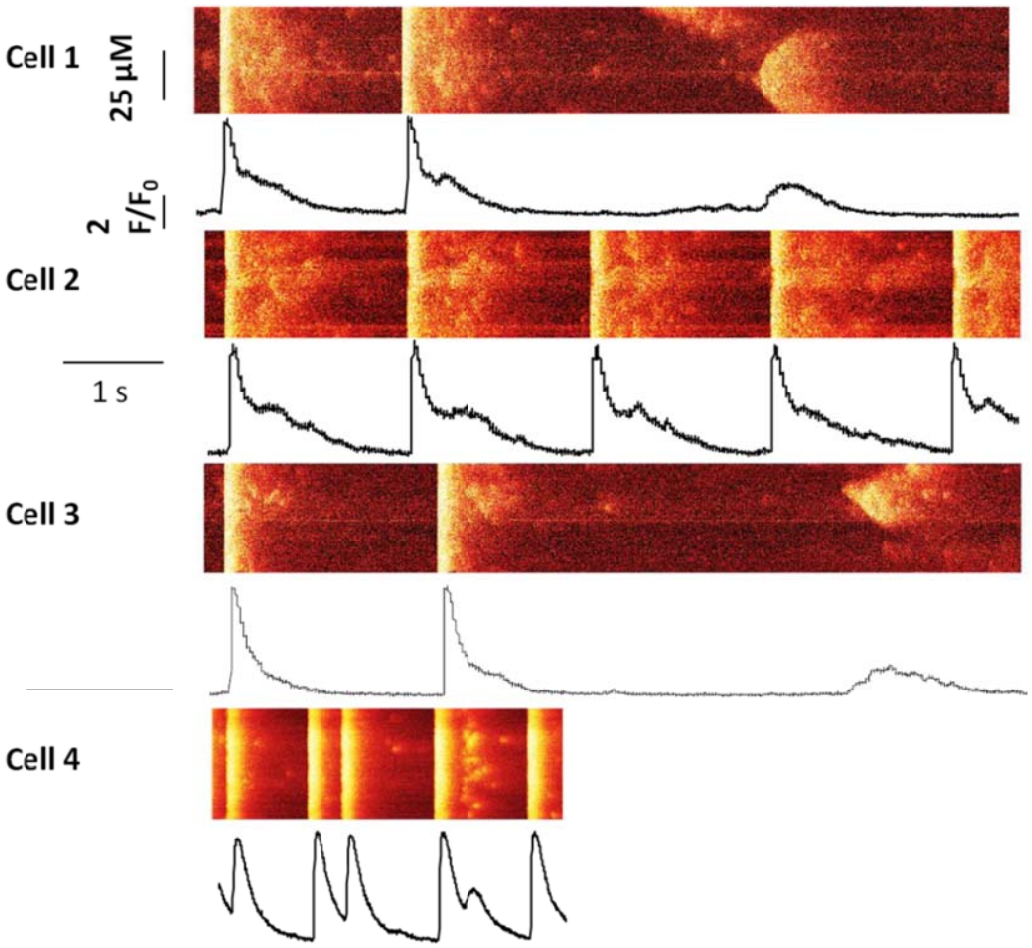

Online Figure II

Online Figure II

Confocal line scan images of R33Q myocytes in the presence of Iso (30 nmol/L). All four cells showed early spontaneous Ca^{2+} releases (sparks or wavelets) which combined slow the global Ca^{2+} transient decay.

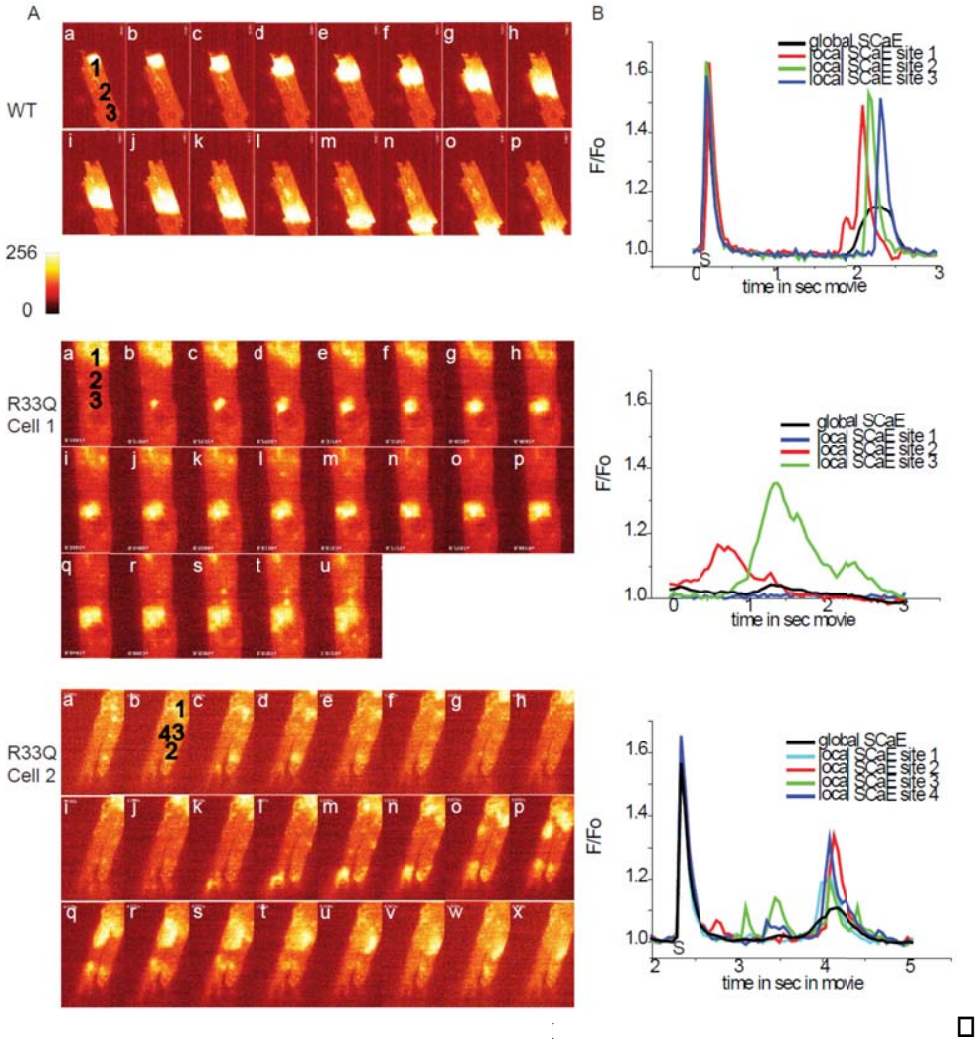

Online Figure III

A. 2D images from movies of one WT and two E33Q cells during spontaneous Ca^{2+} release and Ca^{2+} waves. Fluorescent changes at several sites in cell are shown in small black numbers and plotted in graphs in Panel B. Note changes during last Stimulated beat (S) are not shown in movie images. **B** three graphs depict the various phenotypes of Ca^{2+} releases in WT (top) and two R33Q cell (middle and bottom plots). WT plot shows sequential activation of sites during a typical cell wide wave. Global transient (measured as average of Ca^{2+}over the entire plane of cell) is represented by the black thick line superimposed. Note in this WT cell, the typical spontaneous Ca^{2+} event is a well-formed after-Ca^{2+} transient that would produce a well-formed DAD. In R33Q cell 1, various sized spontaneous Ca^{2+} events (at sites 2,3) are seen at differing times during the sequence. Also note at one site (1) no spontaneous Ca^{2+} events are seen. Notably the global Ca^{2+} transient for cell 1 is small and long lasting. These small Ca^{2+} events would be expected to form a long lasting cell depolarization. In R33Q cell 2, various sized, random Ca^{2+} release events are seen. Some of them developed small propagating waves while others failed to travel across the cell. As a result, the global transient is long lasting and has a small amplitude.

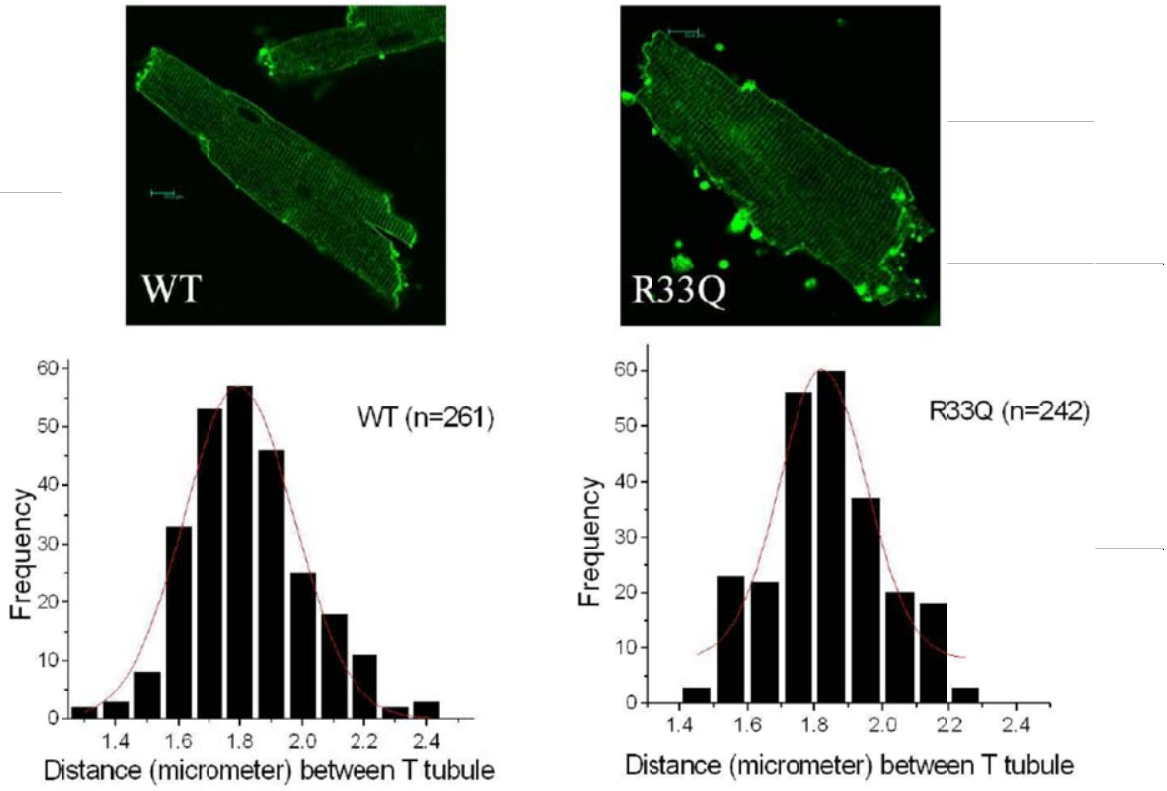

e IV

Online Figure IV

T tubule staining by di-4-ANEPPS in WT and R33Q myocytes. Distribution of the intervals between T tubules in WT myocytes (n=261, N=7 cells) and R33Q myocytes (n=242, N=5 cells). There was no difference of distance between T tubules in WT and R33Q myocytes. The average spatial distance between T tubules was 1.83±0.01 μm in WT myocytes, and 1.83±0.01 μm in R33Q myocytes (P>0.05).

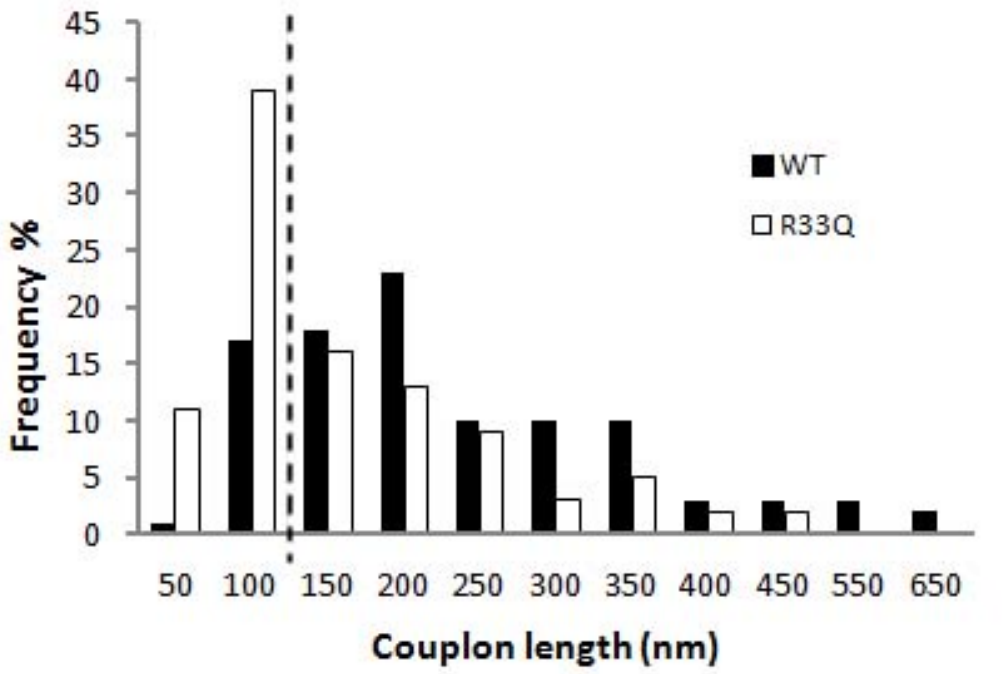

Online figure V

Online Figure V

The bars represent the distribution of the length of couplons in R33Q cardiac cells and in WT cells. The white bars representing the distribution of length of couplons in R33Q myocytes are shifted to the left and approximately 50% of them are shorter than 100 nm as compared to the length of couplons in WT cells.

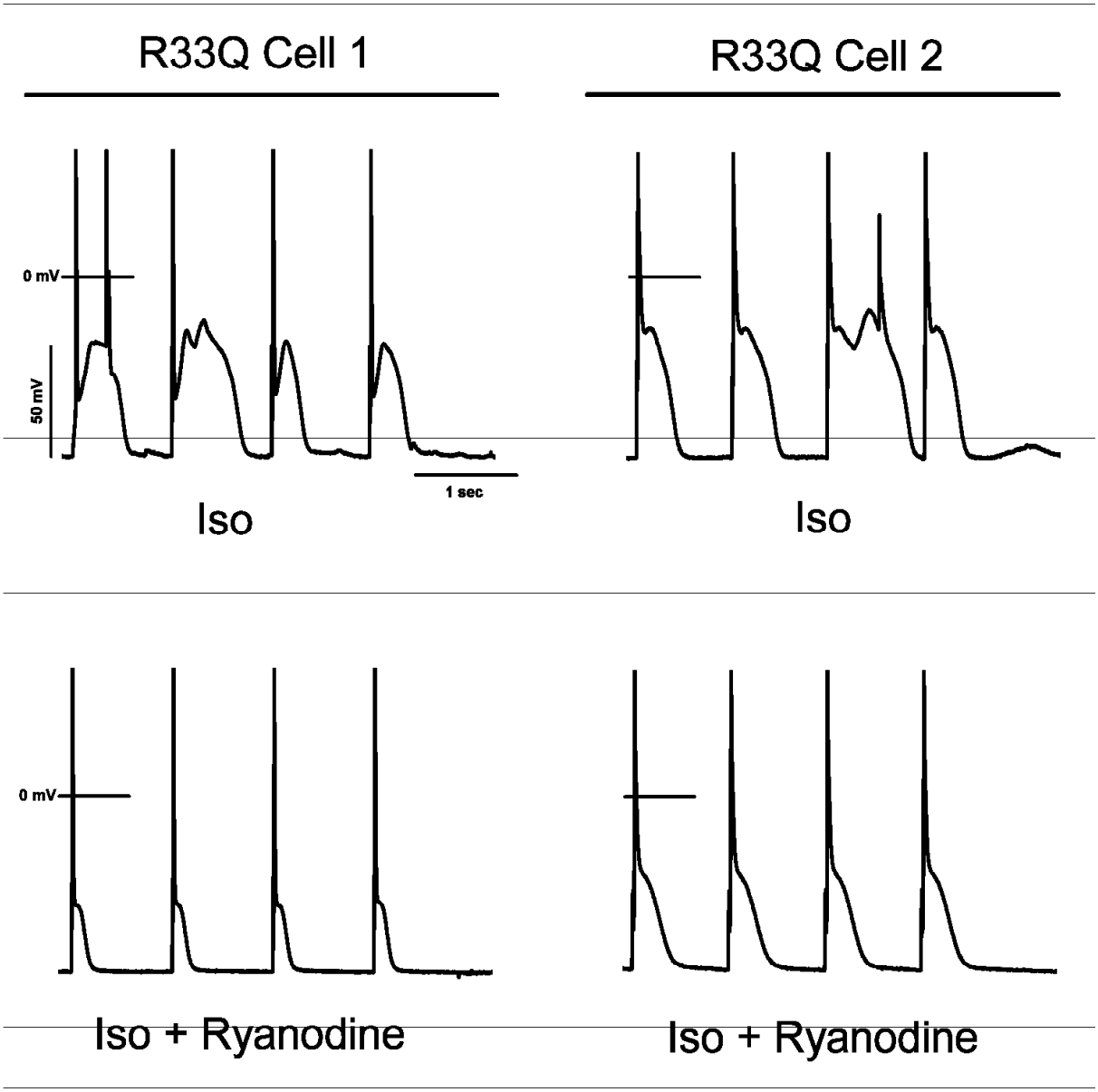

Online figure VI

Online Figure VI

Action potential recordings obtained from two different R33Q myocytes. *Top:* Early afterdepolarizations (EADs) and membrane voltage oscillations induced by administration of isoproterenol 30 nmol/L at 1 Hz pacing stimulus. *Bottom*: Both EADs and membrane voltage oscillations were completely abolished after administration of Ryanodine 10 μmol/L (n=6).

References

1. Liu N, Colombi B, Memmi M, Zissimopoulos S, Rizzi N, Negri S, Imbriani M, Napolitano C, Lai FA, Priori SG. Arrhythmogenesis in Catecholaminergic Polymorphic Ventricular Tachycardia. Insights From a RyR2 R4496C Knock-In Mouse Model. *Circulation Research*. 2006;99:292-298.
2. Picht E, Zima AV, Blatter LA, Bers DM. SparkMaster: automated calcium spark analysis with ImageJ. *Am J Physiol Cell Physiol*. 2007;293:C1073-1081.
3. Thomsen MB, Verduyn SC, Stengl M, Beekman JD, de Pater G, van Opstal J, Volders PG, Vos MA. Increased short-term variability of repolarization predicts d-sotalol-induced torsades de pointes in dogs. *Circulation*. 2004;110:2453-2459.
4. Hilliard FA, Steele DS, Laver D, Yang Z, Le Marchand SJ, Chopra N, Piston DW, Huke S, Knollmann BC. Flecainide inhibits arrhythmogenic Ca2+ waves by open state block of ryanodine receptor Ca2+ release channels and reduction of Ca2+ spark mass. *J Mol Cell Cardiol*. 2009;48:293-301.